Supplementary Information

0D Chiral Hybrid Indium(III) Halides for Second Harmonic Generation

Siming Qi,[a] Fei Ge,[a] Xiao Han,[a] Puxin Cheng,[a] Rongchao Shi,[a] Chao Liu,[a] Yongshen Zheng,[a] Mingyang Xin,[a] Jialiang Xu*[a]

School of Materials Science and Engineering, National Institute for Advanced Materials, Nankai University, Tongyan Road 38, Tianjin 300350, P. R. China

E-mail: jialiang.xu@nankai.edu.cn

Table S1. Crystal Data and Structure Refinement for (*R*-/*S*-MPEA)$_6$InCl$_9$.

Compound	**(*R*-MPEA)$_6$InCl$_9$**	**(*S*-MPEA)$_6$InCl$_9$**
Empirical formula	$C_{54}H_{84}N_6Cl_9In$	$C_{54}H_{84}N_6Cl_9In$
Crystal system	Trigonal	Trigonal
Space group	$P3_221$	$P3_121$
Formula weight	1251.14	1251.14
Temperature (K)	120	100
Wavelength (Å)	1.54184	0.71073
D_{calc} (mg/m^3)	1.253	1.269
Z	6	6
Z'	1	1
a (Å)	17.05090(10)	17.0073(2)
b (Å)	17.05090(10)	17.0073(2)
c (Å)	39.5214(4)	39.2070(6)
α (º)	90	90
β (º)	90	90
γ (º)	120	120
V (Å^3)	9950.79(15)	9821.2(3)
GOF	1.034	1.037

F(000)	3912	3912
$R1[I>2\sigma(I)]$	0.0419	0.0415
$wR2[I>2\sigma(I)]$	0.1211	0.1188
Flack parameter	-0.011(2)	0.0415
CCDC number	2161725	2161726

Table S2. Selected bond angles for (R-MPEA)$_6$InCl$_9$.

Atom	**Atom**	**Atom**	**Angle/ °**
Cl1	In1	Cl2	90.69
Cl1	In1	Cl3	89.82
Cl1	In1	Cl5	88.86
Cl1	In1	Cl6	90.10
Cl4	In1	Cl2	89.43
Cl4	In1	Cl3	89.98
Cl4	In1	Cl5	91.01
Cl4	In1	Cl6	90.11
Cl2	In1	Cl3	88.86
Cl2	In1	Cl6	90.09
Cl5	In1	Cl3	89.22
Cl5	In1	Cl6	91.84

Table S3. Selected bond lengths for (R-MPEA)$_6$InCl$_9$.

Atom	**Atom**	**Length/ Å**
In1	Cl1	2.519
In1	Cl2	2.509
In1	Cl3	2.538
In1	Cl4	2.512
In1	Cl5	2.498

In1	Cl6	2.504

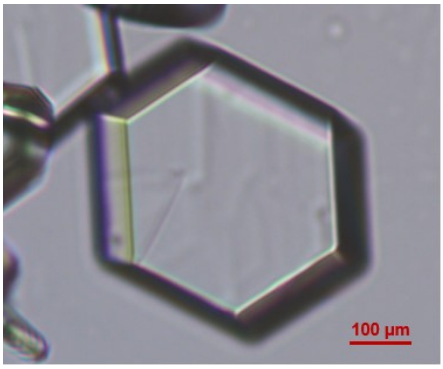

Figure S1. The optical microscope image of (*R*-/*S*-MPEA)$_6$InCl$_9$ crystal in polarized optical micrograph.

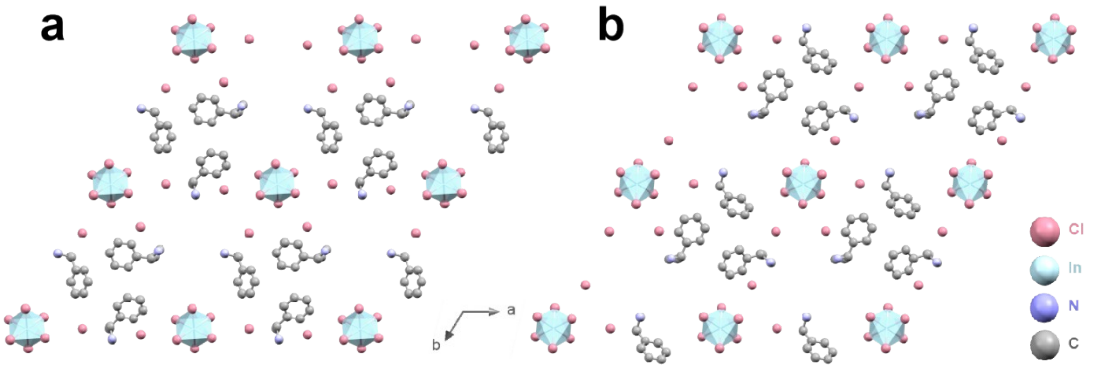

Figure S2. Crystallographic structure diagram of the 0D chiral hybrid Indium halides. View of the structure of (a) (*R*-MPEA)$_6$InCl$_9$ and (b) (*S*-MPEA)$_6$InCl$_9$ along the crystallographic *c*-axis.

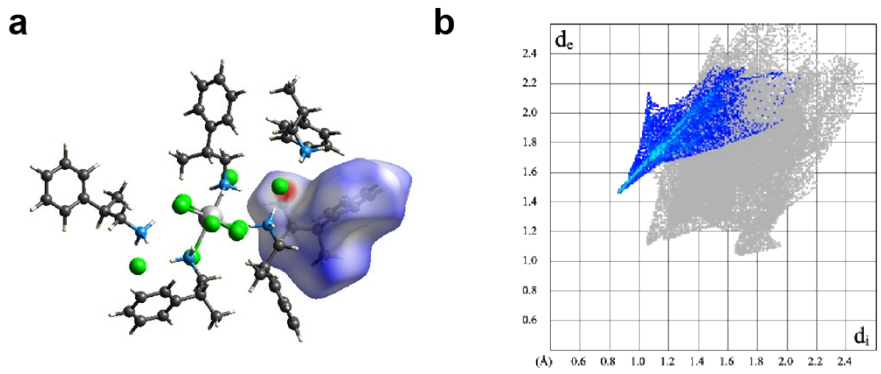

Figure S3. (a) Hirshfeld d_{norm} surfaces in (*R*-MPEA)$_6$InCl$_9$. (b) 2D fingerprint plots in (*R*-MPEA)$_6$InCl$_9$.

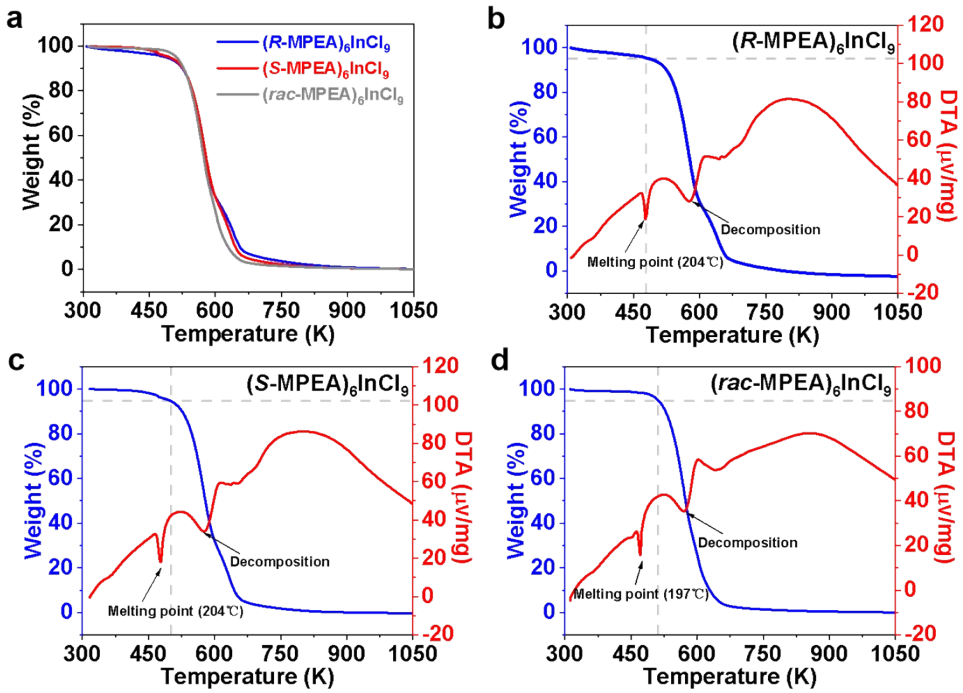

Figure S4. TG-DTA spectra of chiral (*R*-/*S*-/*rac*-MPEA)$_6$InCl$_9$ crystals.

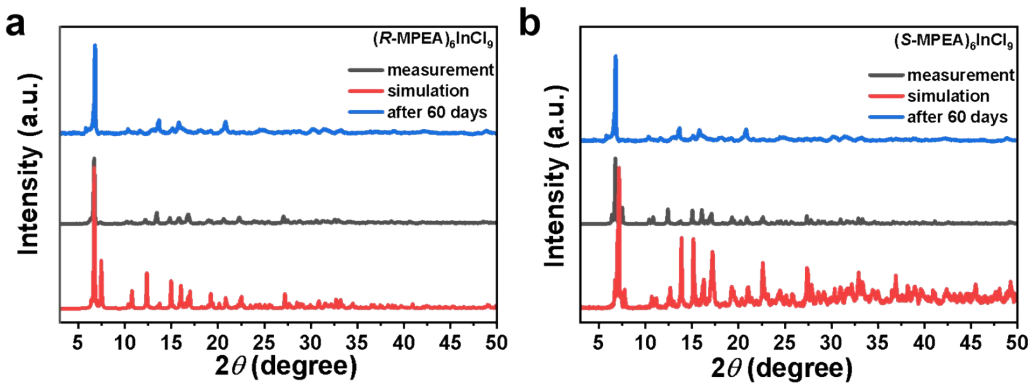

Figure S5. PXRD patterns of chiral (a) (*R*-MPEA)$_6$InCl$_9$ and (b) (*S*-MPEA)$_6$InCl$_9$ crystals.

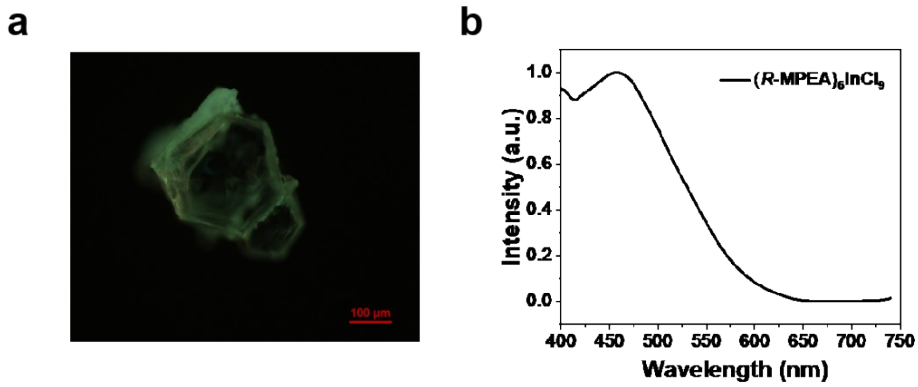

Figure S6. (a) The FL microscope image of chiral (*R*-/*S*-MPEA)$_6$InCl$_9$ crystal taken by the fluorescence microscope. (b) The fluorescence spectrum of chiral (*R*-/*S*-MPEA)$_6$InCl$_9$ crystal.

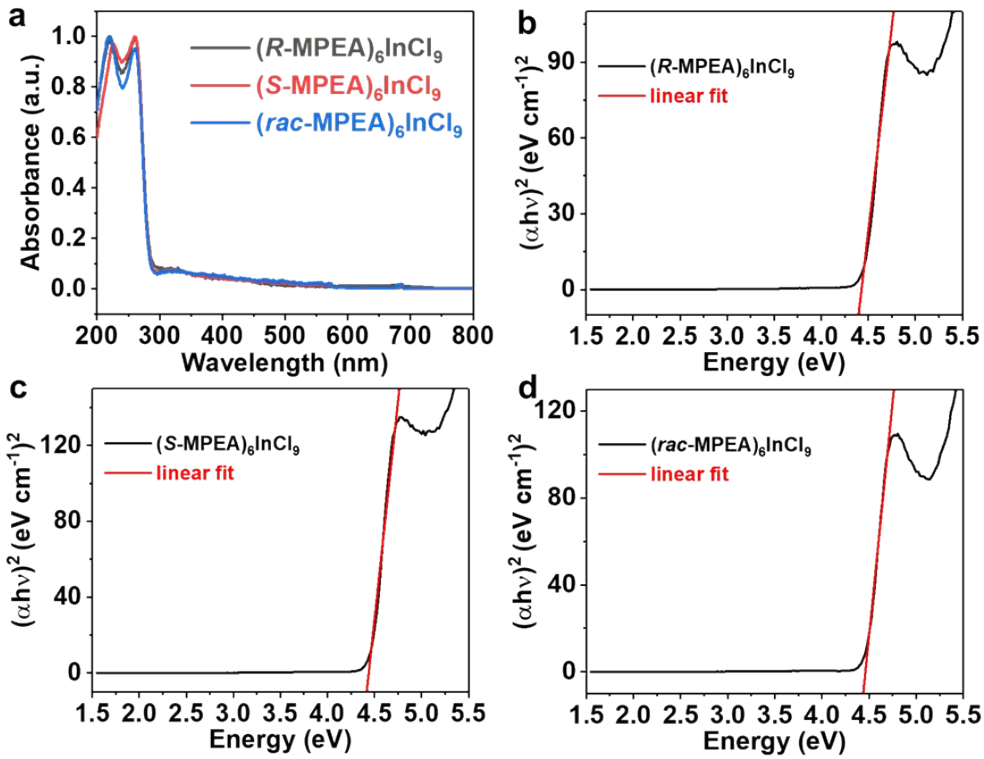

Figure S7. The DRS and Tauc plot of chiral (*R*-/*S*-/*rac*-MPEA)$_6$InCl$_9$ crystal.

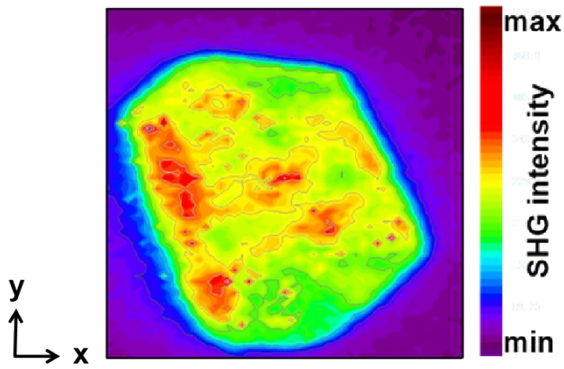

Figure S8. The mapping image of the SHG intensity from a (*R*-MPEA)$_6$InCl$_9$ single crystal (scanning area: x × y = 3.2 × 2.5 mm^2).

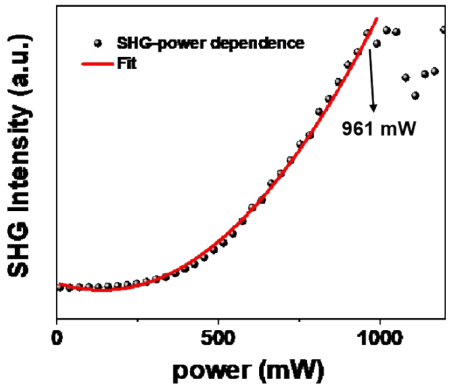

Figure S9. Power dependence of SHG from (*R*-MPEA)$_6$InCl$_9$ single crystal, in which LDT is ~3.82 mJ cm^{-2} (pumped at 800 nm, pulse width: 100 fs, the laser spot of 20 µm in diameter).